Low Temperature Physics/Fizika Nizkikh Temperatur, 2021, vol. 47, No. 1, pp. 29–37

Resonant impurity level of Ni in the valence band of $Pb_{1-x}Sn_xTe$ alloys

E. P. Skipetrov[1,2], N. S. Konstantinov[1], E. V. Bogdanov[1], A. V. Knotko[2,3], and V. E. Slynko[4]

[1]*Faculty of Physics, Lomonosov Moscow State University, Moscow 119991, Russia*

[2]*Faculty of Material Sciences, Lomonosov Moscow State University, Moscow 119991, Russia*

[3]*Faculty of Chemistry, Lomonosov Moscow State University, Moscow 119991, Russia*

[4]*Frantsevich Institute for Problems of Materials Science of NAS of Ukraine, Chernivtsi 58001, Ukraine*
E-mail: skip@mig.phys.msu.ru

Received September 15, 2020, published online November 24, 2020

The phase and elemental compositions and galvanomagnetic properties (4.2 K ≤ T ≤ 300 K, B ≤ 0.07 T) of samples from a single-crystal $Pb_{1-x-y}Sn_xNi_yTe$ ingot (x = 0.08, y = 0.01) synthesized by the Bridgman–Stockbarger method were studied. Microscopic inclusions enriched in nickel were found. It is shown that in the main phase, the tin concentration increases exponentially along the ingot (x = 0.06–0.165), while the concentration of nickel impurity does not exceed 0.4 mol %. A significant increase in the concentration of holes along the ingot and an abnormal increase in the Hall coefficient with increasing temperature were found; both are due to the pinning of the Fermi level by the resonant nickel level located in the valence band. The dependences of the hole concentration and of the Fermi energy at T = 4.2 K on the tin concentration in alloys are calculated using the two-band Kane dispersion law. A qualitative model of electronic structure rearrangement is proposed. The model takes into account the movement of the nickel level into the depth of the valence band with an increase in tin concentration and the redistribution of electrons between the valence band and the level. The energy position of the nickel level and the speed of its movement relative to the top of the valence band with an increase in the tin content in $Pb_{1-x}Sn_xTe$ alloys are estimated.

Keywords: $Pb_{1-x}Sn_xTe$ alloys, 3d transition metal impurities, galvanomagnetic effects, resonant level of nickel.

1. Introduction

Lead telluride and alloys based on it have been widely used for several decades to manufacture thermoelectric devices operating in the medium temperature range (500–900 K) [1–5]. Usually, the efficiency of using semiconductors as thermoelectric materials is estimated by the dimensionless combination of their parameters and temperature $ZT = \sigma S^2 T/\kappa$ (σ is the specific electrical conductivity, S is the Seebeck coefficient, κ is the sum of the coefficients of electronic and phonon thermal conductivity, T is the absolute temperature). To increase ZT, one has to increase the electrical conductivity σ and the Seebeck coefficient S and reduce the thermal conductivity of the material κ. However, since these parameters are not independent, the potential of this traditional approach to optimizing the parameters of thermoelectric materials is now almost exhausted after its extensive application for several decades.

In the last decade, several new promising directions for designing new thermoelectric materials and improving their thermoelectric efficiency have been proposed, in particular, the so-called “band engineering” [4–9]. This direction is based on the phenomenon of a significant increase in the Seebeck coefficient with an increase in the density of electronic states at the Fermi level as a result of a particular modification of the band structure of a semiconductor. Currently, the practical implementation of this general idea in alloys based on lead telluride is possible in three main cases. First, when the extremes of the “light” and “heavy” valence bands located at points L and Σ of the Brillouin zone converge and cross with variations in temperature, with the composition of alloys ($PbTe_{1-x}(Se,S)_x$, $Pb_{1-x}Mg_xTe(Se)$, $Pb_{1-x}Mn_xTe$, …) and with the degree of doping with a number of impurities [6–13]. The coincidence of the Fermi level with the top of the “heavy” valence band leads to a sharp increase in the density of states

at the Fermi level due to particularly large values of the effective mass of holes and of the degree of degeneracy of the valence band extrema at the points Σ of the Brillouin zone. Second, when a sharp peak of the density of resonant impurity states appears in the vicinity of the Fermi level due to doping with group III impurities, transition or rare earth elements (Tl, Cr, Yb, ...) [14–20]. And finally, the first two approaches can be combined to obtain the maximum synergistic effect of increasing the thermoelectric efficiency. This may be realized by achieving the convergence and intersection of the resonant impurity level, which stabilizes the Fermi level in the "light" valence band, with the "heavy" valence band varying the impurity type, matrix composition, and temperature.

In the latter case, new promising materials are SnTe and its alloys doped with In [21–26] as well as $Pb_{1-x}Sn_xTe$ alloys doped with impurities from the second half of a series of 3*d* transition metals (Fe, Co, Ni, Cu) [27–29]. In these semiconductors, resonant impurity levels at low temperatures are or may be located in the valence band in the vicinity of the edges of the "heavy" and "light" valence bands, respectively. In particular, in PbTe, the resonant level of Fe at $T = 4.2$ K is just below the top of the "light" valence band at points *L* of the Brillouin zone [30–32], but with an increase in the tin content in $Pb_{1-x}Sn_xTe$ moves down and approaches the top of the Σ-band [27–29]. The resonant levels of Co and Ni in PbTe seem to be located in the vicinity of the band gap [33–37], but their exact location and movement pattern when changing the composition of PbTe-based alloys are still unknown.

In this paper, the galvanomagnetic properties of $Pb_{1-x}Sn_xTe$ alloys doped with Ni are studied under variations in the matrix composition and impurity concentration. The main objectives of the study were to detect qualitative effects indicating the appearance of an impurity level with doping and pinning of the Fermi level by this level, to determine its energy position, and to build a diagram of the movement of the level relative to the extremes of the valence bands with an increase in the concentration of tin in alloys.

2. Synthesis and composition of samples. Measurement technique

A single-crystal $Pb_{1-x-y}Sn_xNi_yTe$ ingot with a nominal content of tin $x = 0.08$ and nickel $y = 0.01$ was synthesized by the vertical Bridgman–Stockbarger method. Crystallization from the melt of a mixture of pre-synthesized PbTe and SnTe (Pb — 99.9999%, Sn — 99.9999%, Te — 99.9999%) with the addition of $NiTe_2$ (Ni — 99.6%) was carried out in a vacuum quartz ampoule at a temperature gradient of 35 °C/cm and the speed of movement of the temperature front of crystallization of 1.5 mm/h. The use of $NiTe_2$ as a component of the growth charge was aimed at improving the solubility of the Ni impurity in the $Pb_{1-x}Sn_xTe$ matrix, assuming that the melting point of this compound, as in the case of Fe impurity [28], is significantly lower than that of the metallic nickel and NiTe compound. The methods of preparation of the initial components and the modes of synthesis of a single crystal are described in detail in [28, 31].

A cylindrical ingot, whose axis roughly coincided with the crystallographic direction <111>, was cut using string cutting perpendicular to the growth axis into 20 disks with a diameter of ~ 11 mm and a thickness of ~ 1.5 mm (Fig. 1). In the following, the disk numbers correspond to the numbers of the samples studied in the work. In this case, large numbers (for example, 20, 18) correspond to the beginning of the ingot, while the small numbers (for example, 4, 2) — to the end of the ingot.

To determine the distribution of tin and nickel along the ingot, as well as the phase composition and uniformity of samples, x-ray fluorescence microanalysis was performed on a high-resolution scanning electron microscope LEO Supra 50 VP (LEO Carl Zeiss SMT Ltd, Germany) with the INCA Energy+ microanalysis system (Oxford Instruments, England). For this purpose, samples similar in shape to rectangular parallelepipeds with characteristic dimensions of ~ 1 mm were extracted from the disks at the temperature of liquid nitrogen. In Fig. 2 microphotographs of cleaved surfaces and the x-ray emission spectra from the sample areas indicated in the photos are presented (the numbers in the photos correspond to the numbers of disks and samples studied in this work). It was found that within the limits of the experimental error, all samples have good uniformity and the main phase occupies almost the entire volume of samples. However, single microscopic inclusions of the second phases were found in a number of samples from the end of the ingot. They are clearly defined microscopic areas or rather well-cut "microcrystals" enriched with nickel (22–27 at. %), which do not have a specific composition, but are close in composition to $(PbSnNi)_2Te_3$.

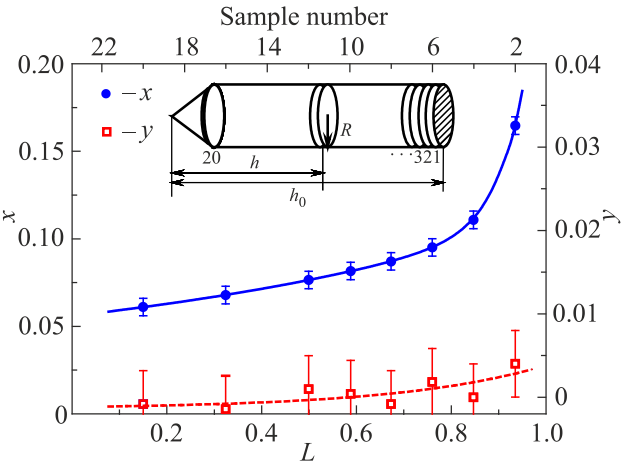

Fig. 1. Distributions of tin and nickel along the length of $Pb_{1-x-y}Sn_xNi_yTe$ ($x = 0.08$, $y = 0.01$) ingot obtained by the x-ray fluorescence microanalysis. The solid curve represents the approximation (1) for Sn distribution.

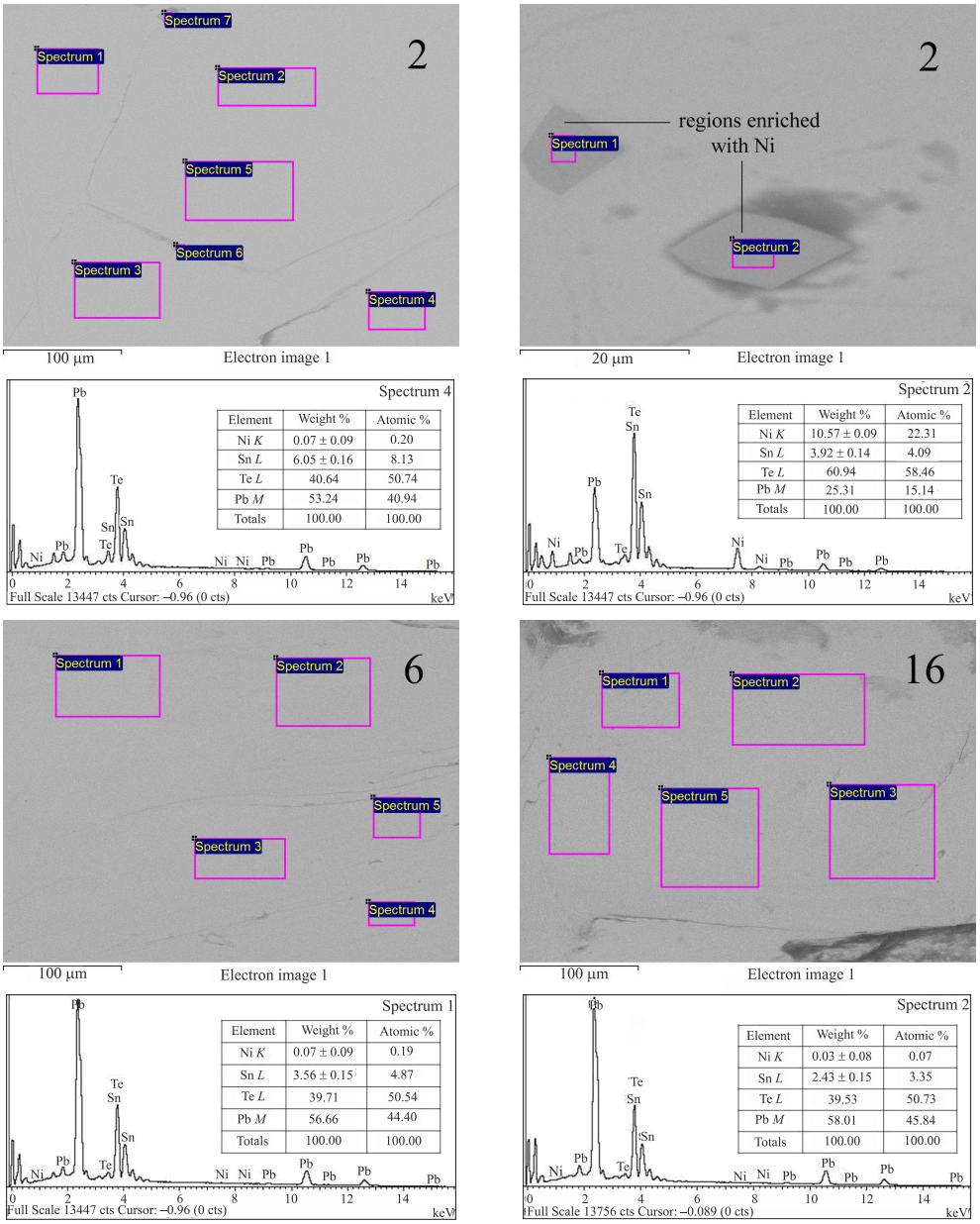

Fig. 2. Microphotographs of the cleaved surfaces and x-ray emission spectra from selected areas for samples 2, 6, and 16 obtained on a scanning electron microscope.

In the main monocrystalline phase, the tin concentration increases monotonously from the beginning to the end of the ingot, covering a range of x values from about 0.06 to 0.165 (see Fig. 1). This behavior is normal and has been observed in almost all previously studied $Pb_{1-x}Sn_xTe$ alloys with 3*d* transition metal impurities. The distribution of tin along the length of the ingot is well approximated using a universal empirical formula obtained for the distribution of substitution impurities in IV–VI semiconductors [38, 39] (solid line in Fig. 1):

$$x = x_0 + A_1 \exp\left(\frac{L}{t_1}\right) + A_2 \exp\left(\frac{L}{t_2}\right). \qquad (1)$$

Here h is the distance from the beginning of the ingot to the middle of the disk, h_0 is the length of the ingot, $L = h/h_0$ is the relative coordinate of the disk, x_0, A_1, A_2, t_1, t_2 are dimensionless fitting parameters. The area under the theoretical distribution curve of tin in the main phase is approximately 0.09, which corresponds well to the integral concentration of tin in the ingot growth charge ($x = 0.08$).

The concentration of nickel impurity also appears to increase along the ingot (see the dashed line in Fig. 1). This is also indirectly evidenced by the appearance of inclusions of the second phase at the end of the ingot. However, the maximum concentration of nickel does not exceed 0.4 mol % with a nominal nickel content of 1 mol % in the ingot growth charge. In addition, almost half of the experimental

points on the $y(L)$ dependence correspond to negative concentration values, and the error in the experimental determination of the nickel concentration for most of the samples was greater than the concentration value itself. Thus, despite the absence of a significant number of microscopic inclusions of other phases, the solubility of nickel impurity seems to be significantly lower than chromium, vanadium, and even iron in $Pb_{1-x}Sn_xTe$ alloys [28, 40] and does not exceed the experimental error of its determination. In this case, it is difficult to construct a real impurity distribution curve along the length of the ingot, and in the future we will only assume that the nickel concentration increases slowly and monotonously along the ingot.

To study the galvanomagnetic effects using an electroerosion machine, samples were cut in the form of rectangular parallelepipeds with characteristic dimensions of 4.0×0.7×0.7 mm. The samples were then etched in a bromine solution in hydrobromic acid and thoroughly washed with ethyl alcohol and distilled water. The electrical contacts to the samples were made of platinum or indium-coated copper wires with a diameter of 0.03 or 0.05 mm, respectively. Current contacts were soldered to the ends of the sample with a micro-soldering iron with In + 4 % Ag + 1 % Au alloy, whereas potential and Hall contacts were welded using an electric spark unit.

The temperature dependences of the resistivity ρ, Hall coefficient R_H, and Hall mobility μ_H in weak magnetic fields (4.2 K ≤ T ≤ 300 K, B ≤ 0.07 T) were studied using a four-probe *dc* method.

3. Composition and temperature dependences of galvanomagnetic parameters

It was found that at liquid-helium temperatures, all the studied samples are characterized by the *p*-type "metallic" conductivity (Figs. 3, 4). As the tin concentration increases along the ingot (from sample 20 to sample 2), the resistivity ρ changes irregularly in a fairly narrow range of values, the Hall coefficient R_H first increases slightly, and then monotonously decreases several times. The dependence of the Hall mobility $\mu_H = R_H/\rho$ on the tin concentration virtually repeats the dependence of $R_H(x)$, and the maximum mobility value does not exceed $3\cdot10^4$ cm^2/(V·s), which is at least an order of magnitude less than the values typical for undoped $Pb_{1-x}Sn_xTe$ alloys [41]. The most important qualitative feature of the composition dependences of the galvanomagnetic parameters of the nickel-doped alloys is a regular and significant (more than by a factor of 6) reduction of the value of the Hall coefficient R_H. It indicates a significant increase in the concentration of free holes in the valence band $p = 1/eR_H$ (e — elementary charge) when the tin concentration increases. Just as in the previously studied $Pb_{1-x-y}Sn_xFe_yTe$ alloys where the concentration of holes in the same range of tin concentrations increases by a factor of 3 [27–29], this may be due to the pinning of the Fermi level by the resonant impurity level and the movement

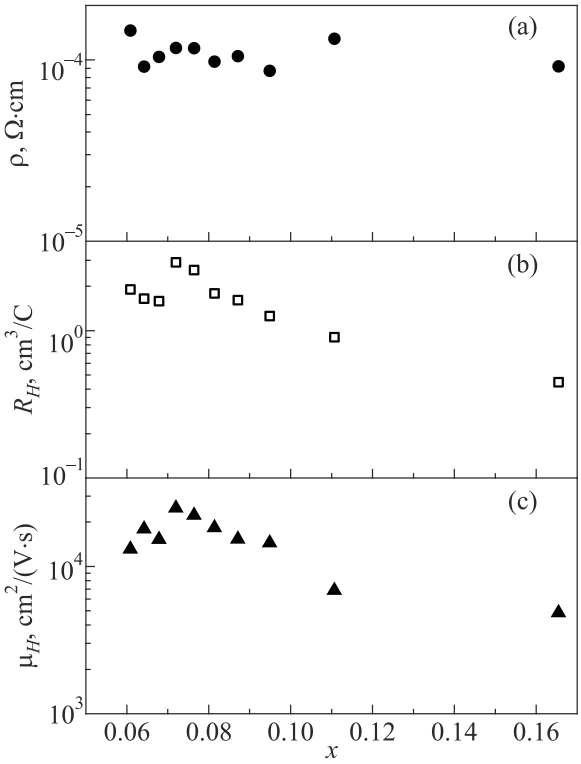

Fig. 3. Galvanomagnetic parameters of $Pb_{1-x-y}Sn_xNi_yTe$ samples at T = 4.2 K as a function of the tin content in alloys.

of this level into the depth of the valence band with an increase in the tin content.

The temperature dependences of the resistivity and Hall mobility of holes in the studied samples have a "metallic" character: when the temperature increases from liquid-helium to room temperatures, the resistivity increases by 1–2 orders of magnitude, and the mobility decreases by about the same factor [see Figs. 3(a) and 3(c)]. In this case, the power-law temperature dependence of mobility at high temperatures ($\mu_H \propto T^{-\alpha}$, α = 2.5–2.8) is due to the preferential scattering of holes on acoustic phonons, characteristic of IV–VI semiconductors [41].

The temperature dependences of the Hall coefficient in all samples are qualitatively similar and anomalous, which is typical for PbTe-based alloys with resonant impurity levels in the electronic spectrum [see Fig. 3(b)]. Upon heating starting from the liquid-helium temperature, the R_H value hardly vary at first but then monotonously increases by a factor of 2–2.5. This effect was previously observed in all lead telluride-based alloys with resonant levels of In [42], Ga [43, 44], Yb [45], Cr [46–48], and Fe [29, 32]. It is believed that it is associated with a decrease in the concentration of free charge carriers taking place when changing the position of the resonant impurity level with respect to the edge of the allowed band and with the redistribution of electrons between the level stabilizing the Fermi level and the band, upon increasing temperature. The magnitude of the effect depends on the position of the resonant level

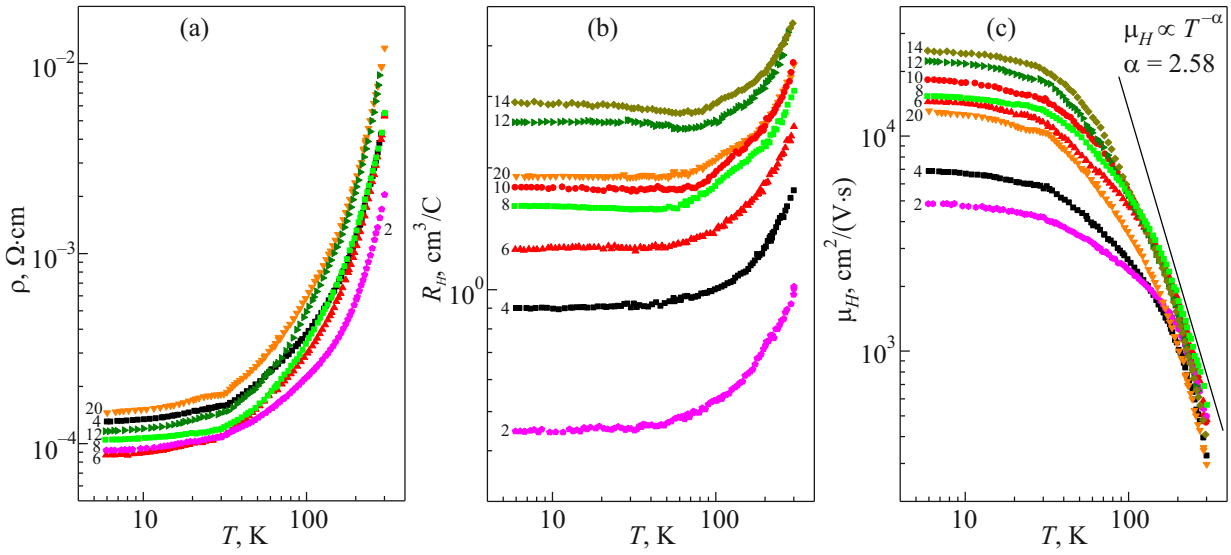

Fig. 4. Temperature dependences of galvanomagnetic parameters in the $Pb_{1-x-y}Sn_xNi_yTe$ alloys (sample numbers are marked).

with respect to the edge of the allowed band (i. e., on the concentration of charge carriers) at liquid-helium temperatures. The maximum increase in R_H (approximately by an order of magnitude) was observed in $Pb_{1-y}Fe_yTe$ with a minimum concentration of holes $p \approx 6 \cdot 10^{17}$ cm^{-3} at $T = 4.2$ K [32]. In our case, the minimum hole concentration at $T = 4.2$ K is several times higher ($p \approx 2 \cdot 10^{18}$ cm^{-3}) and the effect is weaker by the same amount while being approximately the same as in the previously studied $Pb_{1-x-y}Sn_xFe_yTe$ alloys with a similar hole concentration [29]. Therefore, we believe that this behavior of the Hall coefficient with increasing temperature can be considered as yet another qualitative evidence of pinning of the Fermi level by the resonant impurity level of Ni located in the valence band of the studied alloys.

4. Discussion of experimental results

The results of the study of galvanomagnetic effects are used to construct dependences of the hole concentration and of the position of the Fermi level at $T = 4.2$ K on the tin concentration in alloys. To this end, we first calculated the hole concentrations in all samples as $p = 1/eR_H$, where e is the elementary charge, under the assumption of degenerate charge carrier statistics and based on the values of the Hall coefficient at the liquid-helium temperature. Then, the position of the Fermi level relative to the valence band top ($E_v - E_F$) was calculated using hole concentration values in the framework of the non-parabolic two-band Kane dispersion law for $Pb_{1-x}Sn_xTe$ alloys [41]. Details of these calculations with parameters of the dispersion law given in [41] are described in detail in [48].

The results of calculations for all the studied samples are shown in Figs. 5 and 6. It is clearly seen that when the tin concentration increases, the hole concentration and the Fermi energy relative to the valence band top first decrease slightly and then rapidly increase, similarly to what was observed in $Pb_{1-x-y}Sn_xFe_yTe$ alloys earlier [27–29]. A qualitative explanation of this behavior can be given based on the electronic spectrum rearrangement models proposed in [27, 28] for $Pb_{1-x-y}Sn_xFe_yTe$ alloys. These models assume a

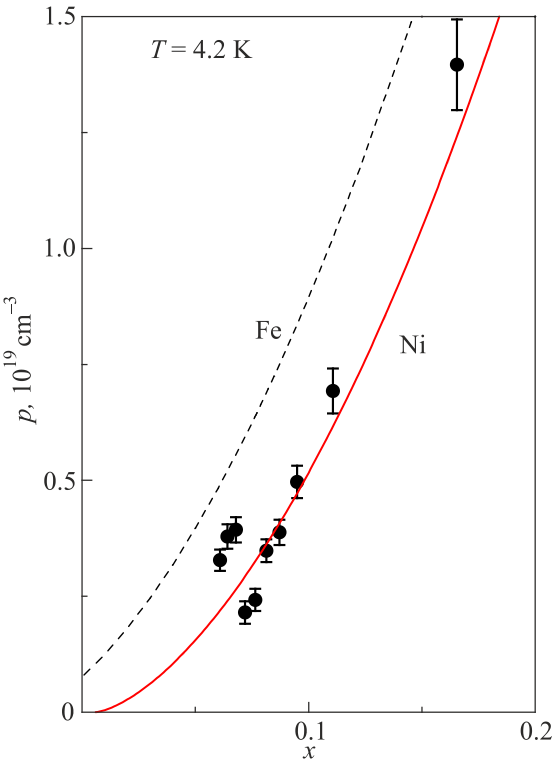

Fig. 5. Dependences of the free hole concentration at $T = 4.2$ K on the tin concentration in $Pb_{1-x-y}Sn_xNi_yTe$ and $Pb_{1-x-y}Sn_xFe_yTe$ alloys (points — experimental data, lines — calculation in the framework of the two-band Kane dispersion law).

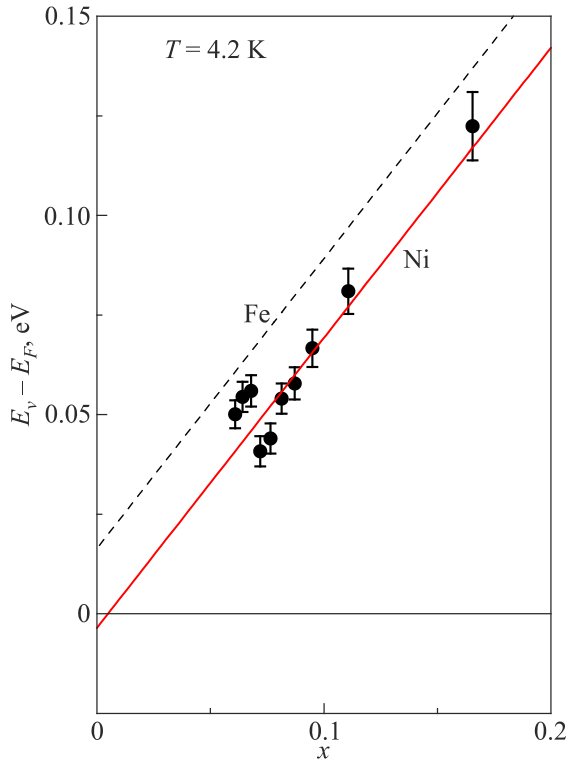

Fig. 6. Dependences of the Fermi level position measured with respect to the top of the valence band at $T = 4.2$ K on the tin concentration in $Pb_{1-x-y}Sn_xNi_yTe$ and $Pb_{1-x-y}Sn_xFe_yTe$ alloys (points — calculation in the framework of the two-band Kane dispersion law, straight lines — approximations by the least squares method).

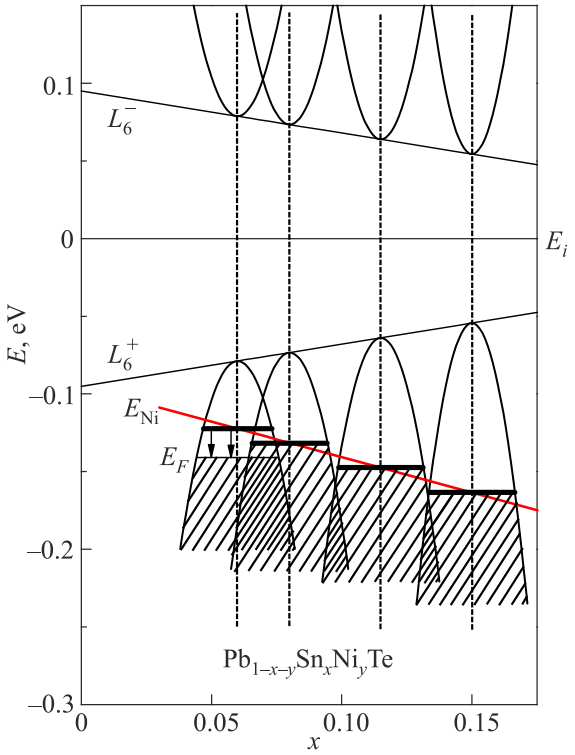

Fig. 7. The qualitative model for rearrangement the electronic structure of $Pb_{1-x-y}Sn_xNi_yTe$ alloys at $T = 4.2$ K with an increase in the concentrations of nickel and tin along the ingot.

flow of electrons from the donor level of iron to the valence band, pinning of the Fermi level by the resonant impurity level, and a shift of the level deep into the valence band with an increase in tin concentration. In addition, we can assume that at the very beginning of the $Pb_{1-x-y}Sn_xNi_yTe$ ingot, the Ni level is located in the valence band slightly above the Fermi level in the samples (Fig. 7). When the concentrations of the donor impurity of nickel and tin increase along the ingot, the gradual filling of the valence band with electrons (i.e., the decrease of the free hole concentration and the shift of the Fermi level up in energy), a shift of the Ni level down in energy (i.e., towards the Fermi level) and pinning of the Fermi level by the Ni resonant level take place. With a further increase in the tin concentration along the ingot, the Ni level stabilizing the Fermi level moves down relative to the top of the valence band, thus inducing a flow of electrons from the valence band to the unoccupied impurity states and a monotonous increase in the hole concentration.

In accordance with this qualitative model of rearrangement of the electronic structure of alloys and by analogy with the case of alloys doped with iron, we assume that the range of alloy compositions in which there is an increase in the concentration of holes and in the Fermi energy relative to the top of the valence band corresponds to the pinning region of the Fermi level by the resonant level of Ni. Then, as in $Pb_{1-x-y}Sn_xFe_yTe$ alloys [27–29], points from the pinning region of the Fermi level on the dependence $(E_v - E_F)(x)$ must fall on a straight line, which is essentially a dependence of the position of the resonant level on the composition of the alloys. However, in contrast to the case of $Pb_{1-x-y}Sn_xFe_yTe$ alloys, this dependence lacks a point at $x = 0$ corresponding to the position of the resonant level in PbTe. This shortage, as well as a significant spread of experimental points in Fig. 6, makes it difficult to independently determine the slope of the line (i. e., the composition coefficient of movement of the Ni level relative to the edge of the valence band) and its intercept yielding the position of the resonant level of Ni in PbTe ($x = 0$).

Taking into account the almost parallel movement of the resonant levels of Cr, V, and Fe with an increase in the concentration of tin in $Pb_{1-x}Sn_xTe$ alloys [27, 28], we assumed that the composition coefficient of movement of the Ni level has approximately the same value as that of the closest to it Fe level: $d(E_v - E_{Fe})/dx \approx 7.3$ meV/mol %. As a result, fixing the slope of the straight line in Fig. 6 and adjusting only the assumed position of the impurity level in PbTe, using the least squares method we obtained the theoretical dependence $(E_v - E_F)(x)$ corresponding to the movement of the resonant level of Ni with increasing tin concentration in alloys (see solid line in Fig. 6). Then, based on this theoretical dependence of the Fermi energy on the composition of alloys and taking into account the pinning of the Fermi level by the resonant level, the theoretical dependence of the hole concentration on the tin concentration $p(x)$

is calculated in the framework of the two-band Kane dispersion law (see solid line in Fig. 5). For comparison, in Figs. 5 and 6 dashed lines represent similar dependences for $Pb_{1-x-y}Sn_xFe_yTe$ alloys studied earlier [27, 28]. It turned out that at liquid-helium temperature in PbTe, the impurity level of Ni is likely to be located near the very top of the valence band and possibly even in the gap. Without claiming high accuracy in determining the energy position of the Ni level relative to the top of the PbTe valence band, we note that this result is in qualitative agreement with the data obtained recently in the study of the galvanomagnetic properties of $Pb_{1-y}Ni_yTe$ alloys [37].

Summing up the results obtained in this paper with the previously obtained data on the position of the resonant levels of other 3*d* transition metals (Cr, V, Fe) in $Pb_{1-x}Sn_xTe$ at $T = 4.2$ K [27, 28], it can also be noted that in the general diagram of the electronic structure rearrangement of $Pb_{1-x}Sn_xTe$ alloys (Fig. 8), the line corresponding to the movement of the Ni level relative to the edges of the energy bands is only slightly higher than the similar line for the Fe level and can cross the top of the "heavy" valence band at $x \approx 0.70$. The proximity of energies of the impurity levels of Fe and Ni is not surprising, since it fully corresponds to the situation in III–V and II–VI semiconductors [49]. Comparison of experimental data on the position of so far known levels of 3*d* transition metals in PbTe and in these well-studied compounds shows that in both cases, when moving along a series of 3*d* transition metal impurities, the impurity levels first shift down in energy (from Sc to Cr), then the Mn level falls deep into the valence band, but the levels from the second half of the series (Fe, Co, Ni, Cu) should return sharply to the top of the valence band or to the gap and be close to each other.

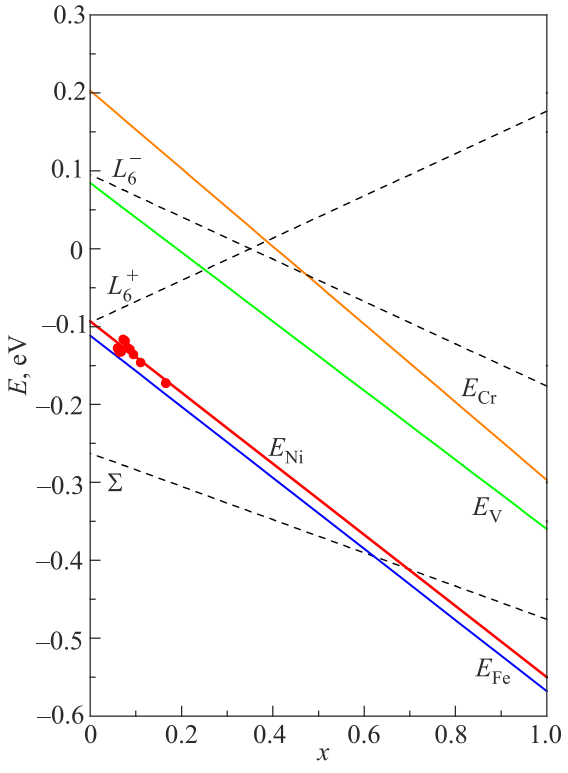

Fig. 8. The general diagram of the electronic structure rearrangement of $Pb_{1-x}Sn_xTe$ alloys doped with 3*d* transition metals (Cr, V, Fe, and Ni) at $T = 4.2$ K with increasing tin concentration.

5. Conclusion

Using scanning electron microscopy and x-ray fluorescence microanalysis, the phase and elemental compositions of samples from $Pb_{1-x-y}Sn_xNi_yTe$ single-crystal ingot ($x = 0.08$, $y = 0.01$) synthesized by the Bridgman–Stockbarger method were studied. It is shown that the tin concentration increases exponentially along the ingot ($x = 0.06$–0.165). The concentration of nickel impurity also seems to increase but does not exceed 0.4 mol %. At the end of the ingot, microscopic inclusions of the second phase, enriched with nickel and close in composition to $(PbSnNi)_2Te_3$, were found.

The galvanomagnetic parameters of samples in weak magnetic fields ($4.2\ \text{K} \le T \le 300\ \text{K}$, $B \le 0.07$ T) were studied under variations in the sample composition. A significant (more than by a factor of 6) increase in the hole concentration at $T = 4.2$ K with an increase in the tin concentration along the ingot and an abnormal increase in the Hall coefficient with an increase in temperature were found, indicating that the Fermi level was pinned by the resonant Ni level located in the valence band. The dependences of the hole concentration and of the Fermi energy relative to the valence band top at $T = 4.2$ K on the tin concentration in alloys are calculated in the framework of the two-band Kane dispersion law.

A qualitative model for rearrangement of the electronic structure of alloys is proposed taking into account the redistribution of electrons between the level and the valence band with doping and due to the motion of Ni resonant level deeper into the valence band with an increase in the tin concentration. Taking into account the similarity of the movement of the resonant levels of the previously studied 3*d* transition metal impurities relative to the edges of the energy bands in $Pb_{1-x}Sn_xTe$, the energy of the resonant level of Ni and the speed of its movement relative to the top of the valence band with an increase in the tin content in $Pb_{1-x}Sn_xTe$ alloys are estimated. It is shown that in PbTe at $T = 4.2$ K, the impurity level of Ni may be in the vicinity of the top of valence *L*-band. As the tin concentration increases, it moves deeper into the valence band, approaches the top of the "heavy" valence Σ-band, and can cross it at the tin concentration $x \approx 0.70$, similarly to the previously studied Fe level.

Acknowledgments

The authors are grateful to B. B. Kovalev (Faculty of Physics, Lomonosov Moscow State University) for his assistance in processing the results of x-ray fluorescence microanalysis.

The work was performed with financial support from the Russian Foundation for Basic Research (project No. 19-02-00774).

1. G. J. Snyder and E. S. Toberer, *Nature Mater.* **7**, 105 (2008).
2. J. R. Soostman, D. Y. Chung, and M. G. Kanatzidis, *Angew. Chem. Int. Ed.* **48**, 8616 (2009).
3. A. V. Dmitriev and I. P. Zvyagin, *Phys. Usp.* **53**, 789 (2010).
4. L.-D. Zhao, V. P. Dravid, and M. G. Kanatzidis, *Energy Environ. Sci.* **7**, 251 (2014).
5. X. Zhang and L.-D. Zhao, *J. Materiomics* **1**, 92 (2015).
6. J. Androulakis, I. Todorov, D.-Y. Chung, S. Ballikaya, G. Wang, C. Uher, and M. Kanatzidis, *Phys. Rev. B* **82**, 115209 (2010).
7. A. D. LaLonde, Y. Pei, H. Wang, and G. J. Snyder, *Mater. Today* **14**, 526 (2011).
8. Y. Pei, X. Shi, A. LaLonde, H. Wang, L. Chen, and G. J. Snyder, *Nature* **473**, 66 (2011).
9. Y. Pei, H. Wang, and G. J. Snyder, *Adv. Mater.* **24**, 6125 (2012).
10. Y. Pei, A. LaLonde, S. Iwanaga, and G. J. Snyder, *Energy Environ. Sci.* **4**, 2085 (2011).
11. Y. Pei, H. Wang, Z. M. Gibbs, A. D. LaLonde, and G. J. Snyder, *NPG Asia Mater.* **4**, e28 (2012).
12. S. A. Yamini, H. Wang, Z. M. Gibbs, Y. Pei, S. X. Dou, and G. J. Snyder, *Phys. Chem. Chem. Phys.* **16**, 1835 (2014).
13. T. Fu, X. Yue, H. Wu, C. Fu, T. Zhu, X. Liu, L. Hu, P. Ying, J. He, and X. Zhao, *J. Materiomics* **2**, 141 (2016).
14. J. P. Heremans, V. Jovovich, E. S. Toberer, A. Saramat, K. Kurosaki, A. Charoenphakdee, S. Yamanaka, and G. J. Snyder, *Science* **321**, 554 (2008).
15. J. P. Heremans, B. Wiendlocha, and A. M. Chamoire, *Energy Environ. Sci.* **5**, 5510 (2012).
16. B. Wiendlocha, *Phys. Rev. B* **97**, 205203 (2018).
17. B. Paul and P. Banerji, *J. Appl. Phys.* **109**, 103710 (2011).
18. B. Paul, P. K. Rawat, and P. Banerji, *Appl. Phys. Lett.* **98**, 262101 (2011).
19. P. K. Rawat, B. Paul, and P. Banerji, *Phys. Status Solidi (RRL)* **6**, 481 (2012).
20. P. K. Rawat, B. Paul, and P. Banerji, *Phys. Chem. Chem. Phys.* **15**, 16686 (2013).
21. G. Tan, F. Shi, S. Hao, H. Chi, L.-D. Zhao, C. Uher, C. Wolverton, V. P. Dravid, and M. G. Kanatzidis, *J. Am. Chem. Soc.* **137**, 5100 (2015).
22. M. Zhou, Z. M. Gibbs, H. Wang, Y. Han, L. Li, and G. J. Snyder, *Appl. Phys. Lett.* **109**, 042102 (2016).
23. L. Wang, X. Tan, G. Liu, J. Xu, H. Shao, B. Yu, H. Jiang, S. Yue, and J. Jiang, *ACS Energy Lett.* **2**, 1203 (2017).
24. D. K. Bhat and U. S. Shenoy, *J. Phys. Chem. C* **121**, 7123 (2017).
25. D. K. Bhat and U. S. Shenoy, *Mater. Today Phys.* **4**, 12 (2018).
26. Xiaofang Tan, G. Liu, J. Xu, Xiaojian Tan, H. Shao, H. Hu, H. Jiang, Y. Lu, and J. Jiang, *J. Materiomics* **4**, 62 (2018).
27. E. P. Skipetrov, B. B. Kovalev, L. A. Skipetrova, A. V. Knotko, and V. E. Slynko, *J. Alloys Compd.* **775**, 769 (2019).
28. E. P. Skipetrov, B. B. Kovalev, L. A. Skipetrova, A. V. Knotko, and V. E. Slynko, *Fiz. Nizk. Temp.* **45**, 233 (2019) [*Low Temp. Phys.* **45**, 201 (2019)].
29. E. P. Skipetrov, B. B. Kovalev, L. A. Skipetrova, A. V. Knotko, and V. E. Slynko, *Semiconductors* **53**, 1419 (2019).
30. E. P. Skipetrov, O. V. Kruleveckaya, L. A. Skipetrova, E. I. Slynko, and V. E. Slynko, *Appl. Phys. Lett.* **105**, 022101 (2014).
31. E. P. Skipetrov, O. V. Kruleveckaya, L. A. Skipetrova, A. V. Knotko, E. I. Slynko, and V. E. Slynko, *J. Appl. Phys.* **118**, 195701 (2015).
32. E. P. Skipetrov, O. V. Kruleveckaya, L. A. Skipetrova, and V. E. Slynko, *J. Appl. Phys.* **121**, 045702 (2017).
33. G. V. Lashkarev, M. V. Radchenko, V. V. Asotskiy, A. V. Brodovoy, A. I. Mirets, and O. I. Tananaeva, *Mater. Sci. Forum* **182-184**, 631 (1995).
34. V. V. Asotskii, T. A. Kuznetsova, G. V. Lashkarev, M. V. Radchenko, O. I. Tananaeva, and V. V. Teterkin, *Semiconductors* **30**, 88 (1996).
35. T. A. Kuznetsova, V. P. Zlomanov, and O. I. Tananaeva, *Inorg. Mater.* **34**, 878 (1998).
36. N. Romcevic, J. Trajic, T. A. Kuznetsova, M. Romcevic, B. Hadzic, and D. R. Khokhlov, *J. Alloys Compd.* **442**, 324 (2007).
37. E. P. Skipetrov, B. B. Kovalev, I. V. Shevchenko, A. V. Knotko, and V. E. Slynko, *Semiconductors* **54**, 1171 (2020).
38. V. E. Slynko and W. Dobrowolski, *Bull. Natl. University "Lviv Polytechnic", Electron.,* No. 681, 144 (2010).
39. E. I. Slynko, V. M. Vodopyanov, A. P. Bakhtinov, V. I. Ivanov, V. E. Slynko, W. Dobrowolski, and V. Domukhowski, *Visn. Lviv Polytec. Natl. Univ., Electron.,* No. 734, 67 (2012).
40. E. P. Skipetrov, A. V. Knotko, E. I. Slynko, and V. E. Slynko, *Fiz. Nizk. Temp.* **41**, 185 (2015) [*Low Temp. Phys.* **41**, 141 (2015)].
41. G. Nimtz and B. Schlicht, *Narrow-Gap Semiconductors*, *Springer Tracts in Modern Physics*, Springer-Verlag, Berlin, Heidelberg, New York, Tokyo (1983), Vol. 98.
42. V. I. Kaidanov and Yu. I. Ravich, *Phys. Usp.* **28**, 31 (1985).
43. E. P. Skipetrov, E. A. Zvereva, N. N. Dmitriev, A. V. Golubev, and V. E. Slynko, *Semiconductors* **40**, 893 (2006).
44. E. P. Skipetrov, N. A. Pichugin, E. I. Slyn'ko, and V. E. Slyn'ko, *Semiconductors* **47**, 729 (2013).
45. E. Skipetrov, E. Zvereva, L. Skipetrova, B. Kovalev, O. Volkova, A. Golubev, and E. Slyn'ko, *Phys. Status Solidi B* **241**, 1100 (2004).
46. M. Ratuszek and M. J. Ratuszek, *J. Phys. Chem. Solidi* **46**, 837 (1985).
47. V. D. Vulchev and L. D. Borisova, *Phys. Status Solidi A* **99**, K53 (1987).
48. E. P. Skipetrov, N. A. Pichugin, E. I. Slyn'ko, and V. E. Slyn'ko, *Fiz. Nizk. Temp.* **37**, 269 (2011) [*Low Temp. Phys.* **37**, 210 (2011)].
49. K. A. Kikoin and V. N. Fleurov, *Transition Metal Impurities in Semiconductors: Electronic Structure and Physical Properties*, World Scientific, Singapore (1994).

Резонансний рівень домішки Ni у валентній зоні сплавів $Pb_{1-x}Sn_xTe$

E. P. Skipetrov, N. S. Konstantinov, E. V. Bogdanov, A. V. Knotko, V. E. Slynko

Вивчено фазовий та елементний склади, а також гальваномагнітні властивості (4,2 K ≤ T ≤ 300 K, B ≤ 0,07 Тл) зразків з монокристалічного злитка $Pb_{1-x-y}Sn_xNi_yTe$ (x = 0,08, y = 0,01), який синтезовано методом Бриджмена–Стокбаргера. Виявлено мікроскопічні вкраплення, які збагачені нікелем. Показано, що в основній фазі концентрація олова експоненціально зростає вздовж злитка (x = 0,06–0,165), тоді як концентрація домішок нікелю не перевищує 0,4 моль %. Виявлено значне збільшення концентрації дірок уздовж злитка та аномальне збільшення коефіцієнта Холла із підвищенням температури; обидва зумовлені закріпленням рівня Фермі резонансним рівнем нікелю, який розташований у валентній зоні. Залежності концентрації дірок та енергії Фермі при T = 4,2 K від концентрації олова в сплавах розраховуються за двосмуговим законом дисперсії Кейна. Запропоновано якісну модель перебудови електронної структури. Модель враховує переміщення рівня нікелю в глибину валентної зони зі збільшенням концентрації олова та перерозподілом електронів між валентною зоною та рівнем. Оцінено енергетичне положення рівня нікелю та швидкість його руху відносно вершини валентної зони зі збільшенням вмісту олова в сплавах $Pb_{1-x}Sn_xTe$.

Ключові слова: сплави $Pb_{1-x}Sn_xTe$, домішки 3d-перехідних металів, гальваномагнітні ефекти, резонансний рівень нікелю.